International Journal of Microwave and Wireless Technologies, 2015, 7(3/4), 287–296.
doi:10.1017/S1759078715000094

RESEARCH PAPER

Highlighting trapping phenomena in microwave GaN HEMTs by low-frequency *S*-parameters

CLÉMENT POTIER[1,2], JEAN-CLAUDE JACQUET[2], CHRISTIAN DUA[2], AUDREY MARTIN[1], MICHEL CAMPOVECCHIO[1], MOURAD OUALLI[2], OLIVIER JARDEL[2], STÉPHANE PIOTROWICZ[2], SYLVAIN LAURENT[1], RAPHAËL AUBRY[2], OLIVIER PATARD[2], PIERO GAMARRA[2], MARIE-ANTOINETTE DI FORTE-POISSON[2], SYLVAIN L. DELAGE[2] AND RAYMOND QUÉRÉ[1]

This paper presents an original characterization method of trapping phenomena in gallium nitride high electron mobility transistors (GaN HEMTs). This method is based on the frequency dispersion of the output-admittance that is characterized by low-frequency S-parameter measurements. As microwave performances of GaN HEMTs are significantly affected by trapping effects, trap characterization is essential for this power technology. The proposed measurement setup and the trap characterization method allow us to determine the activation energy Ea and the capture cross-section σ_n of the identified traps. Three original characterizations are presented here to investigate the particular effects of bias, ageing, and light, respectively. These measurements are illustrated through different technologies such as AlGaN/GaN and InAlN/GaN HEMTs with non-intentionally doped or carbon doped GaN buffer layers. The extracted trap signatures are intended to provide an efficient feedback to the technology developments

Keywords: Circuit design and applications, Si-based devices and IC technologies, Microwave Measurements, Modelling, Simulation and characterizations of devices and circuits, Technologies and Devices (III-V, nano, quantum, opto)

Received 29 October 2014; Revised 08 January 2015; Accepted 11 January 2015; first published online 5 February 2015

I. INTRODUCTION

The very high potential of gallium nitride (GaN) high electron mobility transistors (HEMTs) at microwave frequencies has already been confirmed through many studies. Moreover, the alloy of indium–aluminum–nitrogen (InAlN), when used in adequate proportions inside the InAlN/GaN HEMT structure, permits a lower strain in the crystal lattice of the barrier layer and to achieve higher current densities compared with the more conventional AlGaN/GaN structure. However, despite the high-voltage and power capabilities of GaN HEMTs, they still have some limitations of their microwave performances.

Indeed, trapping phenomena are still present in GaN devices due to physical defects such as those induced by dislocations, atoms incorporation (intentionally or not), dandling bonds, etc. These physical defects are responsible for degradations in microwave performances, such as power slump, or even complex bias current variations and ACPR degradation in the case of modulated signals [1]. Thus, the knowledge and understanding of these technological defects are critical for improving the quality and consequently the electrical behavior of GaN HEMTs.

Several characterization techniques of traps already exist [2, 3] but the proposed method, which is based on vector network analyzer (VNA) measurements, presents some key advantages: it is precise because it features a wide dynamic range; it can reveal signal variations in one sweep over a large frequency scale; it performs on-wafer measurements of low-frequency *S*-parameters and the temperature can be completely mastered.

These measurements are used to determine the activation energy E_a and the capture cross-section σ_n of the identified traps from the low-frequency dispersion of the output admittance. In addition to other measurements like pulsed *I*–*V* or load-pull measurements, this method can also be used to improve and validate the nonlinear electrical models of trapping effects [4, 5] in GaN HEMTs.

In this paper, Section II describes the identification method of trap parameters and its illustration through the simulation of a physical InAlN/GaN HEMT model including a predefined trap. Section III presents the developed measurement setup and the characterization techniques that were implemented to investigate the particular impacts of bias, ageing, and light on the trapping behavior. These measurements were performed on three different InAlN/GaN and AlGaN/

[1]XLIM – UMR 7252, Université de Limoges/CNRS, 87060 Limoges Cedex, France. Phone: +33 160 403 024
[2]III-V Lab, 91461 Marcoussis Cedex, France
Corresponding author:
C. Potier
Email: clement.potier@xlim.fr

GaN technologies. Finally, the conclusion discusses the issues pointed out in the previous section with regard to the impacts of bias voltage, ageing, and light exposure on the trapping behavior.

II. PRINCIPLE OF TRAP CHARACTERIZATION FROM LOW-FREQUENCY DISPERSION OF THE OUTPUT ADMITTANCE

A) Simplified small-signal HEMT model including one trap

The principle of this characterization method is to investigate the trapping behavior of GaN HEMTs by measuring the low-frequency dispersion of their output admittance Y_{22} [6, 7], which can be related to the emission rate. Since the emission rate of traps changes with temperature, this characterization is performed at different temperatures and the Arrhenius' law is used to extract the trap signatures from the temperature dependence of Y_{22} measurements.

Figure 1 shows how the low-frequency dispersion of Y_{22}, which is due to a single trap with an emission time constant τ_n, can be modeled by an additional parasitic network (g_n, C_n) at the output of the small-signal HEMT model [8, 9].

At low frequencies, the output admittance Y_{22} simplifies to:

$$Y_{22} = \left(g_d + \frac{g_n(\omega\tau_n)^2}{1+(\omega\tau_n)^2}\right) + j\frac{g_n(\omega\tau_n)}{1+(\omega\tau_n)^2} \quad \text{with} \quad \tau_n = \frac{C_n}{g_n}. \tag{1}$$

Calculations on derivative forms of the real and imaginary parts of Y_{22} equation (1) show that the emission time constant τ_n of the active trap can be extracted from the frequencies f_{Rinf} and f_{Ipeak} that correspond to the inflexion points of $real[Y_{22}]$ and the peaks of $imag[Y_{22}]$, respectively. Indeed, the frequencies f_{Rinf} and f_{Ipeak} can be derived from (1) and written as

$$f_{Rinf} = f_{\text{Real}[Y_{22}]\text{ at inflexion point}} = \frac{1}{2\pi\sqrt{3}\tau_n}, \tag{2}$$

$$f_{Ipeak} = f_{\text{Imag}[Y_{22}]\text{ at peak point}} = \frac{1}{2\pi\tau_n}. \tag{3}$$

The number of peaks of $imag[Y_{22}]$ or the number of inflexion points of $real[Y_{22}]$ reflects the number of traps. As it will be illustrated through measurements in Section III, the extraction of frequencies f_{Ipeak} from the peaks of $imag[Y_{22}]$ is more convenient and precise than the extraction of frequencies f_{Rinf} from the inflexion points of $real[Y_{22}]$.

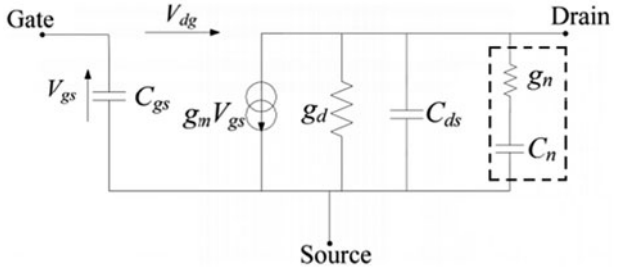

Fig. 1. Small-signal HEMT model including one trap (g_n, C_n).

As the capture time constant of a trap is much smaller than its emission time constant, the capture time constant can be neglected at low frequencies. The emission rate follows the Arrhenius' law and increases with temperature. Indeed, if the emission rate increases, the emission time constant τ_n decreases, and thus the peak value of $imag[Y_{22}]$ is shifted toward higher frequencies as indicated by (3). Therefore, the measured evolution of f_{Ipeak} with the temperature allows us to determine the activation energy E_a and the capture cross-section σ_n by using the Arrhenius' equation written as

$$\frac{e_n}{T^2} = \frac{\sigma_n A_n}{g}\exp\left(-\frac{E_a}{kT}\right), \tag{4}$$

$$\text{with } A_n = \frac{N_c\ v_{th}}{T^2} \text{ and } e_n = \frac{1}{\tau_n},$$

where e_n is the emission rate, T is the temperature, σ_n is the capture cross-section, N_c is the effective density of states for electrons in the conduction band, v_{th} is the thermal velocity, g is the degeneracy factor, E_a is the apparent activation energy, and k is the Boltzmann constant.

As indicated in (5), the natural logarithm of the Arrhenius' equation (4) shows that a plot of $ln(\tau_n T^2)$ versus $(kT)^{-1}$ gives a straight line whose slope is equal to the apparent activation energy E_a, while its y-intercept can be used to determine the capture cross-section σ_n.

$$\ln(\tau_n T^2) = \frac{E_a}{kT} - \ln\left(\frac{\sigma_n A_n}{g}\right). \tag{5}$$

Therefore, the trap signatures can be extracted from the measured imaginary part of Y_{22} at low frequencies and its dependence on the temperature.

B) Physical simulations

To illustrate the principle of this electrical measurement method for trapping characterizations, physical simulations were performed using the Silvaco ATLAS code for an InAlN/AlN/GaN/SiC HEMT device structure. Shockley–Read–Hall and Fermi–Dirac statistics were enabled while the effects of self-heating and impact ionization were not implemented in these simulations. The surface potential and the polarization charge at the InAlN/AlN and AlN/GaN interfaces were adjusted in the physical model to match the measured pinch-off voltage, sheet resistance and DC transconductance of our device.

The physical simulation was defined to study only the impact of traps located in the buffer region on the small-signal parameters. In the physical model, no trap was implemented for the moment on the surface region, neither in the barrier nor at the layer interfaces. Therefore, both acceptor and donor traps were defined and added inside the GaN buffer with an identical capture cross-section set to 10^{-15} cm^2. Acceptor and donor traps were located at 0.9 eV from the valence band energy and 0.3 eV from the conduction band energy, respectively. The acceptor and donor trap densities were fixed at 5×10^{16} cm^{-3} and 2×10^{16} cm^{-3}, respectively.

https://doi.org/10.1017/S1759078715000094 Published online by Cambridge University Press

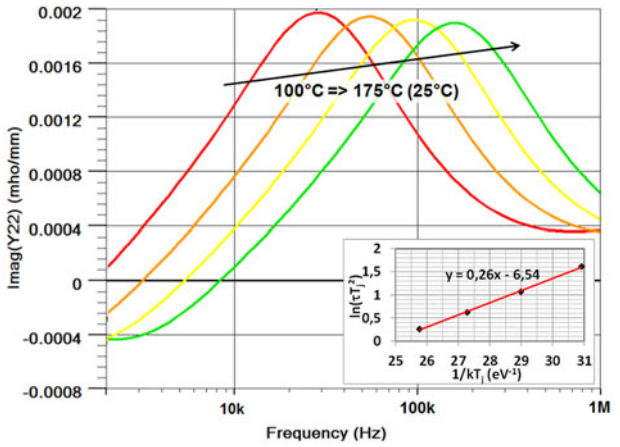

Fig. 2. Imaginary part of Y_{22} versus frequency derived from a physical simulation at various ambient temperatures. The inset shows the Arrhenius plot with an extracted activation energy of 0.26 eV [7].

Using this physical model with predefined trap values, a small-signal simulation was performed using Silvaco ATLAS and the imaginary part of Y_{22} was extracted. These results of a physical simulation are intended to be used as measurement results for the proposed extraction technique. Figure 2 shows the imaginary part of Y_{22} simulated at different ambient temperatures ranging from 100 to 175°C. The corresponding Arrhenius plot is shown in the inset of Fig. 2. From this plot, we extracted activation energy of 0.26 eV that corresponds to the donor energy level of 0.3 eV entered for the physical simulation.

However, we did not succeed to detect the acceptor trap and more simulations are needed to investigate this issue.

This physical simulation confirms qualitatively the apparent activation energy that can be extracted from the low-frequency dispersion of the output admittance Y_{22} and its measured dependence on temperature.

III. EXPERIMENTAL WORK

This section presents some measurement results to illustrate the trap characterization method based on the low-frequency dispersion of Y_{22} versus temperature.

The measurement setup developed for the trapping characterization is shown in Fig. 3. A low-frequency to high-frequency (LF–HF) vector network analyzer (Agilent E5061B-3L5 [10]) is connected in one-port configuration to the drain terminal of the device for measuring its Y_{22} parameter. The network analyzer can operate from 5 Hz up to 3 GHz and integrates its own bias system allowing 100 mA current and 40 V, while the gate port is biased by an external DC voltage source. All measurements are performed on-wafer and the probe station is equipped with a thermal chuck allowing a temperature range from −65 to 200°C. The on-wafer calibration of the vector network analyzer is performed using a classical SOLT method.

As trapping effects have long emission time constants, the measurements presented in this section were performed from 10 Hz to 10 MHz with a filter bandwidth of 5 Hz and ambient temperatures ranging from 25 to 170°C. The next subsections present the characterization techniques that were implemented to investigate the particular impacts of bias, ageing and light on the trapping behavior. This section is essentially dedicated to the measurement results while the next section will be dedicated to a discussion on the measured impacts.

This experimental work was performed on three different GaN HEMT technologies grown on SiC substrate by low-pressure metal-organic chemical vapor deposition. Ohmic contacts of Ti/Al/Ni/Au multilayer showed a typical resistance of 0.45 Ω.mm. The Argon ion implantation was used for device isolation and Ni/Pt/Au T-gates were realized. The devices were passivated with a 250-nm-thick Si_3N_4 layer deposited by plasma enhanced chemical vapor deposition.

A) Measured impact of the drain voltage on trap parameters

The measured impact of the drain bias voltage on trap parameters is illustrated here through a 2 × 50 μm carbon doped InAlN/GaN HEMT grown on SiC with 250-nm gate length. This device was fabricated using a 3-inch reactor. The heterostructure consists in 1.8-μm-thick carbon doped GaN buffer layer, 1-nm AlN spacer layer, and 8-nm undoped $In_{0.19}Al_{0.81}N$ barrier layer with 18.7% of indium content, giving rise to InAlN barrier layer close to lattice-matched conditions to GaN.

The device was first characterized at a drain bias voltage V_{DS} of 21 V and a drain current density I_{DS} of 100 mA/mm. Figures. 4 and 5 show the measured real and imaginary parts of Y_{22} versus frequency and temperature. Both figures demonstrate a positive dispersion of f_{Rinf} and f_{Ipeak} toward high frequencies when the temperature increases.

It is clear from the Figs. 4 and 5, that the peaks of $imag[Y_{22}]$ are more precisely determined than the inflexion points of $real[Y_{22}]$, both methods giving τ_n, as explained in Section II. Therefore, the frequencies f_{Ipeak} corresponding to the measured peak values of $imag[Y_{22}]$ at each temperature are used to determine the temperature dependence of the emission time constant τ_n.

At this first drain bias voltage V_{DS} of 21 V, Fig. 5 shows that each measured curve of $imag[Y_{22}]$ at a given temperature presents two peaks that reveal the presence of two traps. Thus, the measured evolution of f_{Ipeak} was extracted from Fig. 5 for both traps to determine the temperature dependence of their emission rate (3). Then, using the Arrhenius' equation, both trap signatures were determined with apparent activation energies

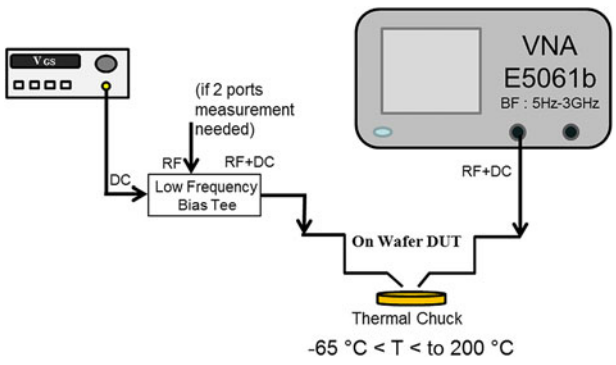

Fig. 3. Schematic of the LF–HF (5–3 GHz) measurement setup in one-port configuration for the characterization of the output admittance [7].

https://doi.org/10.1017/S1759078715000094 Published online by Cambridge University Press

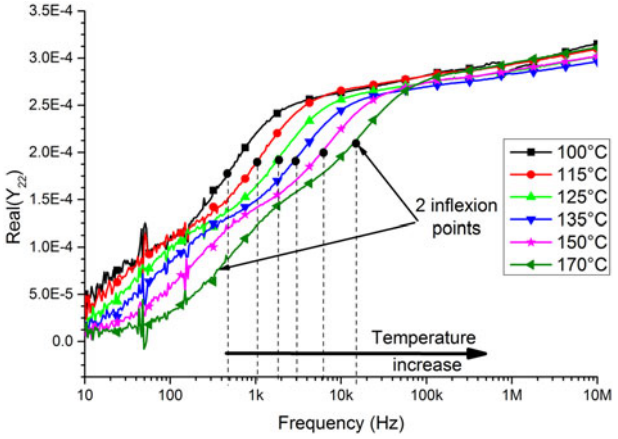

Fig. 4. Measured real part of Y_{22} versus frequency in the temperature range 25–170°C. Dashed lines show the inflexion points for one trap.

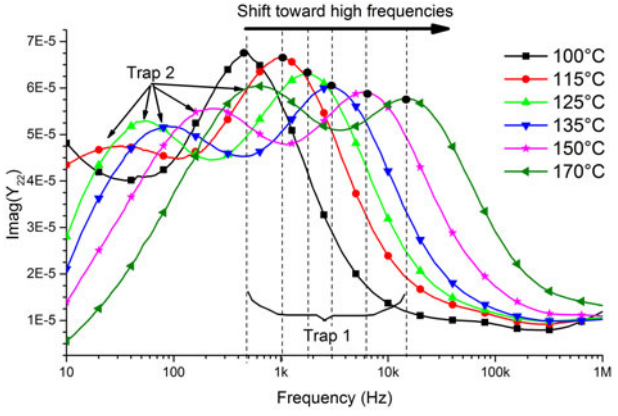

Fig. 5. Measured imaginary part of Y_{22} versus frequency in the temperature range 25–170°C. The arrow shows the shift of peak values toward high frequencies with increasing temperature.

E_a of 0.8 and 1.02 eV, respectively, and capture cross-sections σ_n of 1.3×10^{-15} cm² and 3.37×10^{-15} cm², respectively. The extracted Arrhenius plots of both traps are shown in Fig. 6.

The elevation of the component's temperature due to the self-heating is taken into account. We previously extracted the thermal resistance of our transistor by using the Ansys

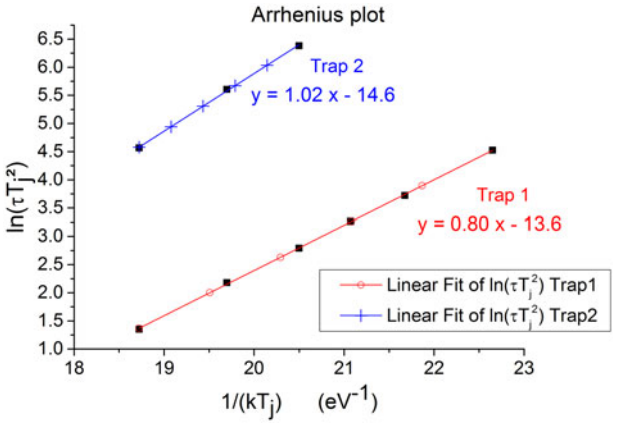

Fig. 6. Arrhenius plots of both traps extracted from Fig. 5.

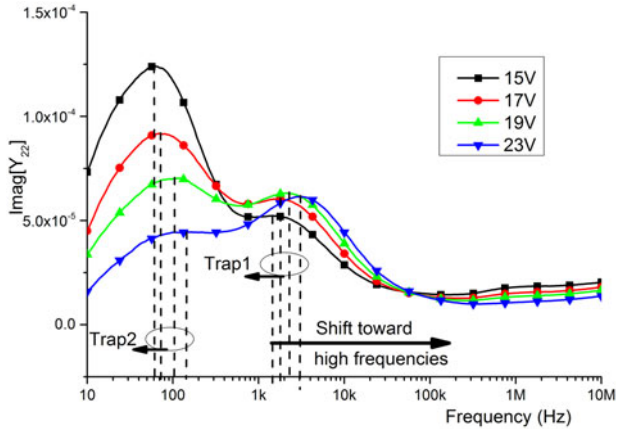

Fig. 7. Measured imag[Y_{22}] versus frequency at a fixed temperature of 135°C for a drain voltage varying from 15 to 23 V. The arrow shows the shift of peak values towards high frequencies with increasing voltage.

software and by applying three-dimensional finite elements simulations. Thus, knowing the thermal resistance R_{th}, the temperature of the thermal chuck T_{chuck} and the dissipated power P_{diss} we were able to extract the junction temperature T_j:

$$T_j = T_{chuck} + R_{th} \times P_{diss}. \quad (6)$$

After these first measurements at a constant voltage of 21 V, a second characterization process was defined to investigate the impact of the electric field on trap parameters. Indeed, as the temperature causes a strong frequency dispersion of Y_{22}, the characterization was defined to separate the impact of the electric field with the thermal effect due to a variation of the drain voltage. Thus, to impose the same thermal state when varying the drain bias voltage V_{DS}, the ambient temperature and the drain bias current I_{DS} were monitored to keep constant the dissipated power during measurements. Finally, at a fixed ambient temperature of 135°C and a fixed DC power of 2.1 W/mm, Fig. 7 shows the measured imaginary part of Y_{22} for a drain voltage V_{DS} varying from 15 to 23 V.

As previously observed in Fig. 5, each measured curve of Fig. 7 at a given V_{DS} voltage shows two peaks of $imag[Y_{22}]$ that characterize two traps. Moreover, when the drain voltage V_{DS} increases, the frequencies f_{1peak} move towards high frequencies, and thus the emission rate increases. Therefore, the emission rate increases not only with the temperature but also with the applied electric field. As shown on the curves of Fig. 7, the magnitude of peaks is also very sensitive to the bias voltage V_{DS}. During this measurement process, it has been observed that this phenomenon saturates for drain voltage lower than 10 V and higher than 25 V, as shown in Fig. 8.

The dependence of the emission rate on the electric field was already observed [11, 12] and could be attributed to Poole–Frenkel effects. This mechanism of field-assisted emission is defined by the Poole–Frenkel equation that relates the variation of the ionization energy E_i to the square root of the applied electric field F

$$E_i(F) = E_i(0) - \beta\sqrt{F} \quad \text{with} \quad \beta = \sqrt{\frac{q^3}{\pi\varepsilon}}, \quad (7)$$

where $E_i(0)$ is the zero-field binding energy of the electron in

https://doi.org/10.1017/S1759078715000094 Published online by Cambridge University Press

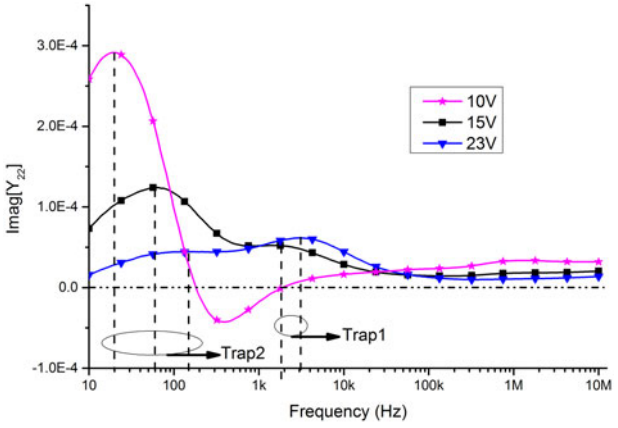

Fig. 8. Bias dependency of the measured imag[Y_{22}] versus frequency at a fixed temperature of 135°C and a fixed dissipated power of 2.1 W/mm for a larger range of the drain bias voltage from 10 to 23 V.

the trap, q is the electron charge, and ε is the dielectric constant of the material.

During this first experimental study at different drain voltages, the trap signatures were extracted and their dependence on the applied voltage was compared with the theoretical Poole–Frenkel mechanism.

On a small range of drain voltage from 21 to 24 V, where the electric field F is assumed proportional to the drain voltage, Fig. 9 plots the extracted apparent activation energy E_a of the first trap (Trap1 in Fig. 7) as a function of the square root of the drain voltage. As a first conclusion for this measured device, Fig. 9 shows that the apparent activation energy increases with the square root of the applied field, which is contrary to the Poole–Frenkel model demonstrating that the Poole–Frenkel mechanism is not the dominant effect in this case.

This first study of Section III dealt with the issue of field-assisted emission through the low-frequency measurements of a 2 × 50 μm carbon doped InAlN/GaN HEMT. For this device, two deep-level traps called trap 1 and trap 2 were characterized in Figs 5 and 6 with activation energies of 0.8 and 1.02 eV, respectively.

Moreover, the measurements performed at different drain voltages clearly demonstrated in Fig. 7 that the extracted activation energies strongly depend on the electric field. This suggests that they are donor traps [13], which are also confirmed by the physical simulations. As previously explained, this also suggests that the Poole–Frenkel effect might be responsible of this field-assisted emission. To assess whether the measured dependence of the activation energy on the applied voltage follows the Poole–Frenkel equation, the apparent activation energies E_a were extracted in Fig. 9 at a fixed thermal state for a small variation range of the drain voltage. Finally, the plot of Fig. 9 shows that the activation energy E_a are quite proportional to the square root of the drain voltage, which would be consistent with the Poole–Frenkel model. However, Fig. 9 shows that the apparent activation energy increases with the square root of the applied voltage, which is contrary to the Poole–Frenkel equation (7). It should be noted that the same measurement process was applied to other similar technologies that demonstrated activation energies decreasing with increasing drain voltage.

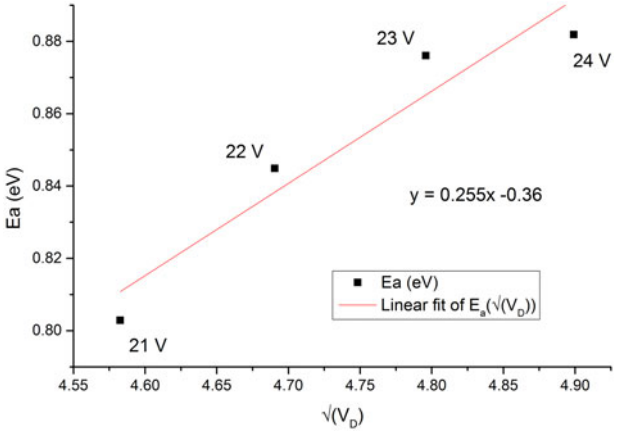

Fig. 9. Extracted apparent activation energies as a function of the square root of the drain voltage V_D ranging from 21 to 24 V (Trap1 of Fig. 7).

As a result, these measurements show that the Poole–Frenkel effect may be one of the physical mechanisms that explain the measured field dependence of trap parameters but it seems that other unidentified mechanisms are also involved.

In addition, it is also interesting to point out that saturation effects are observed when the applied field is too low or too high. As shown in Fig. 8, we can notice that the shape of $imag[Y_{22}]$ at the lower drain voltage of 10 V was clearly modified with even a reverse peak that goes into negative value. Finally, Fig. 8 shows that the peak of $imag[Y_{22}]$ tends to disappear at low V_{DS} voltages below 10 V, and thus the zero-field activation energy cannot be directly extracted. This demonstrates that the simplified RC model of traps can only explain the positive peaks and shows its limitations in the cases of low fields or interactions between several traps.

B) Measured impact of ageing on trap characteristics

The measurement of ageing effects and their impact on trap characteristics are illustrated here through a 2 × 250 μm non-intentionally doped InAlN/GaN HEMT grown on SiC substrate with 150-nm gate length. This device was fabricated using a 2-inch reactor. The heterostructure consists in 1.7-μm-thick non-intentionally doped GaN buffer layer, 1-nm AlN spacer layer, and 11.5-nm undoped $In_{0.18}Al_{0.82}N$ barrier layer.

Two procedures of ageing were performed during ~4000 h on two device samples by applying a DC stress of 25 V drain voltage and 237 mA/mm current density. During this DC stress, the two devices were set at high ambient temperatures of 225°C (case 1) and 330°C (case 2), respectively.

To quantify the classical impact of ageing on drain currents, I–V measurements were periodically performed during the ageing time. As shown in Fig. 10, we can note a quick decrease of the measured current at the beginning of ageing, and thereafter the negative impact on the drain current is gradually reduced.

Moreover, to assess the impact of ageing on the trapping behavior of devices, after-stress low-frequency measurements were performed in three cases of ageing. The first two cases of ageing correspond to cases 1 and 2 of DC stress during

https://doi.org/10.1017/S1759078715000094 Published online by Cambridge University Press

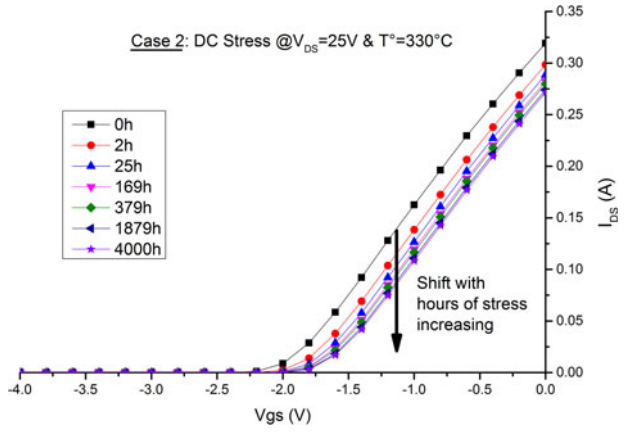

Fig. 10. Measured drain current I_{DS} versus the gate voltage V_{GS} during the ageing caused by a DC stress of 25 V and 237 mA/mm at a temperature of 330°C. The arrow shows the decrease of current with the ageing time.

~4000 h, as previously described above. The third case corresponds to an unstressed device.

Figure 11 shows the after-stress measurements of $imag[Y_{22}]$ under 20-V drain voltage and 100-mA/mm current density at four ambient temperatures of 35, 60, 85, and 135°C. When comparing the after-stress low-frequency measurements of unstressed and stressed devices, this characterization demonstrates the strong impact of ageing on trap behaviors.

In the case of the after-stress measurement at an ambient temperature of 85°C, three vertical dashed lines of Fig. 11 point to the peaks of $imag[Y_{22}]$ that correspond to the three cases of ageing. This helps to illustrate that the frequency f_{Ipeak} is shifted towards low frequencies when we move from the peak of the unstressed device towards that of the worst case of stressed device (case 2). The same observation applies to each temperature of Fig. 11 indicating that the emission rate decreases with ageing. In addition, not only the peak frequencies f_{Ipeak} but also the peak magnitudes decrease with increasing stress.

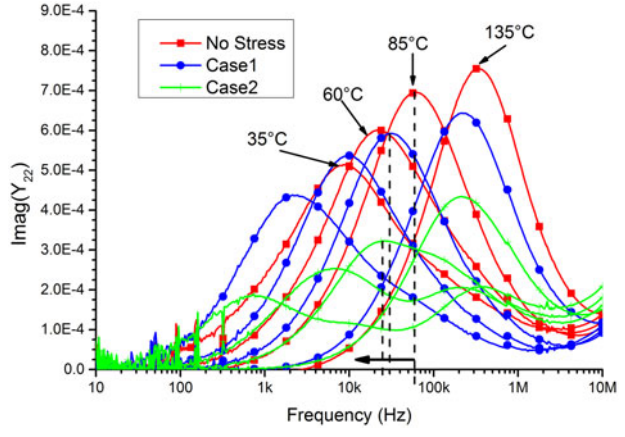

Fig. 11. Comparison between measured imag$[Y_{22}]$ of stressed and unstressed devices. Cases 1 and 2 correspond to 4000 h ageing with a DC stress of 25 V and 237 mA/mm at 225 and 330°C, respectively. After-stress measurements were performed under (20 V, 100 mA/mm) at the temperatures of 35, 60, 85, and 135°C. At 85°C, the dashed lines show the shift of f_{Ipeak} toward low frequencies from the unstressed case to cases 1 and 2.

Moreover, the after-stress measurements of Fig. 11 clearly show that a second peak appears in the worst case of stressed device (case 2). This is particularly evident from the measured curve of case 2 at 35°C.

This second study of Section III dealt with the measured impact of ageing on trap parameters for a 2 × 250 μm non-intentionally doped InAlN/GaN HEMT. Two identical device samples were exposed to a DC stress of 25-V drain voltage and 237-mA/mm current density during ~4000 h at high ambient temperatures of 225°C (case 1) and 330°C (case 2), respectively. *I–V* measurements were first reported to illustrate the impact of ageing [14] with a decrease of 15% for the maximum current and a shift of 0.25 V for the pinch-off voltage after 380 h of ageing.

To evaluate the impact of ageing on trap characteristics, after-stress low-frequency measurements of $imag[Y_{22}]$ were performed versus temperature on the two stressed devices and compared to that of an unstressed device. These after-stress measurements of Fig. 11 clearly demonstrate the strong impact of ageing on trap behaviors. In addition, it was observed that the emission rate decreases with ageing for this particular device with a second peak appearing in the worst case of stressed device (case 2). This shows that low-frequency measurements of $imag[Y_{22}]$ can be very helpful to assess whether some extracted traps are responsible for stronger post-stress degradation and to witness the creation of new traps due to this stress. This would be very useful for the reliability work of technology developments. It should be noted that the low-frequency measurement technique is well suited for reliability measurements because of its dynamic range and speed.

C) Measured impact of light on trap parameters

The impact of light on trap characteristics is illustrated through low-frequency measurements of a 2 × 250 μm non-intentionally doped AlGaN/GaN HEMT grown on SiC substrate with 0.7-μm gate length. This device was fabricated using a 3-inch reactor. The heterostructure consists in 1.7-μm-thick non-intentionally doped GaN buffer layer and 26.6-nm undoped $Al_{0.19}Ga_{0.81}N$ barrier layer.

During initial on-wafer *I–V* measurements, the active devices of this wafer were found to be very sensitive to light exposure. Figure 12 shows on-wafer *I–V* measurements of gate and drain current densities versus the gate voltage in the cases of dark conditions or light exposure. In both cases, the measured drain currents were identical above pinch-off. However, near the pinch-off region, Fig. 12 shows that the drain current density increased dramatically when the device was exposed to light coming from a fluorescent lamp. In this case, the light exposure was responsible for the degradation of pinch-off characteristics.

Thereafter, the impact of light exposure on the trapping behavior was characterized by low-frequency measurements of Y_{22} to assess whether particular trapping effects are responsible for this high level of light sensitivity.

Figure 13 shows the comparison between measured $imag[Y_{22}]$ with and without light exposure at an ambient temperature of 135°C under bias conditions of 20-V drain voltage and 100-mA/mm drain current density. In the case of light exposure, it can be observed that a distinct peak appears at

https://doi.org/10.1017/S1759078715000094 Published online by Cambridge University Press

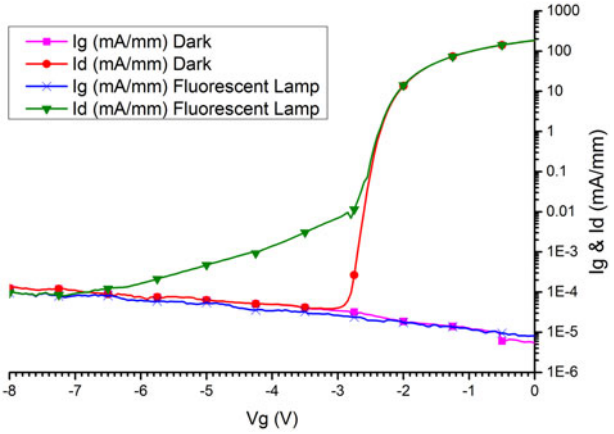

Fig. 12. Comparison between measured drain and gate current densities (I_D and I_G) versus the gate voltage V_G under dark conditions or light exposure from a fluorescent lamp.

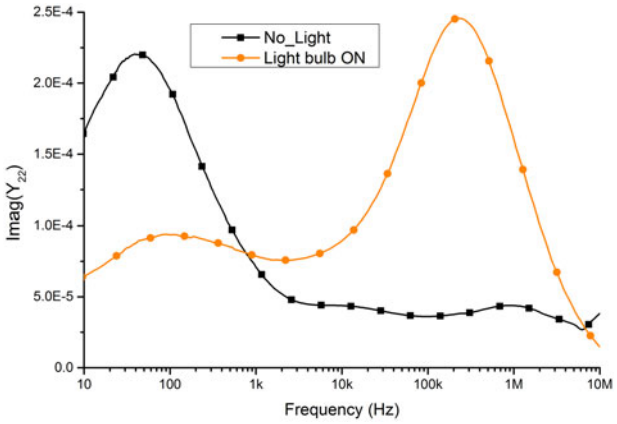

Fig. 13. Comparison between measured imag[Y_{22}] versus frequency with and without light exposure. The device is biased under 20-V drain voltage and 100-mA/mm drain current density at an ambient temperature of 135°C.

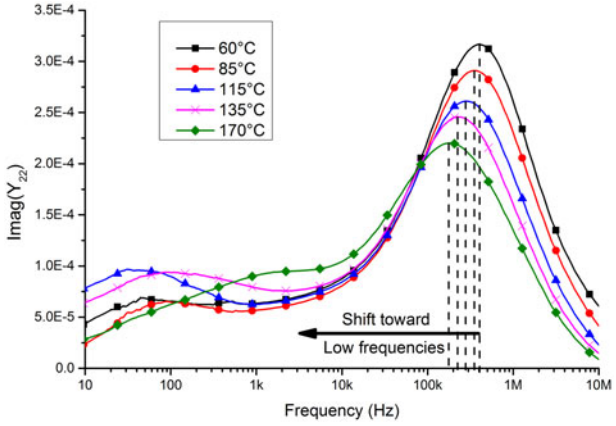

Fig. 14. Measured imag[Y_{22}] versus frequency with light exposure in the temperature range 60–170°C. The arrow shows the shift of peak values towards low frequencies with increasing temperature.

a significantly higher frequency, while the peak that was previously observed at a lower frequency under dark conditions is greatly decreased. Therefore, temperature measurements were performed with light exposure to extract this trap signature.

Figure 14 shows the measured *imag*[Y_{22}] with light exposure at ambient temperatures ranging from 60 to 170°C under the same bias conditions of 20 V drain voltage and 100 mA/mm drain current density. One can clearly observe that the measured behavior of this trap is opposite to that observed in the previous cases. Indeed, the frequency f_{1peak} of Fig. 14 is shifted toward low frequencies with increasing temperature, and thus the emission rate is decreased.

As a result of this, the Arrhenius plot extracted from the measured temperature dependence of Fig. 14 still gives a straight line, but with a negative slope, and thus a negative value of −0.18 eV for the extracted activation energy E_a.

This third experimental study reported in Section III dealt with the impact of light on the trap parameters of a 2 × 250 µm non-intentionally doped AlGaN/GaN HEMT. Indeed, initial on-wafer *I*–*V* measurements of this particular device demonstrated a high sensitivity to light exposure with a great increase of the drain current from 40 µA to 10 mA near the pinch-off voltage. Thus, low-frequency measurements were performed with and without light exposure to investigate the role of traps in this light sensitivity. Figure 13 demonstrates that the degradation of drain current can be clearly attributed to a specific trap that appears with the light exposure. Indeed, a trap is initially detected at low frequencies under dark conditions, while its magnitude is greatly reduced with light exposure, which reveals another trap at higher frequencies.

Thus, temperature measurements were performed with light exposure to extract the signature of this trap activated by the light. In this case, Fig. 14 shows that the emission rate of this trap decreases with increasing temperature, which is opposite to the most commonly observed behavior. Indeed, this might be explained by the characteristic of an acceptor-like trap instead of a donor-like trap [15]. A future experimental work is planned to determine what wavelength is responsible for this trap activation using LEDs of different colors associated to a monochromator for illuminating the device.

IV. CONCLUSION

This paper reports the characterization principle of trapping effects in GaN HEMTs by low-frequency measurements of their output-admittance versus temperature. The extraction technique of activation energies and capture cross-sections for detected traps is based on the Arrhenius equation applied to temperature-dependent measurements of the imaginary part of Y_{22}. The extraction principle of trap signatures from low-frequency measurements was qualitatively validated in Section II through the simulation of an actual physical model, which integrated a predefined trap. In Section III, the particular impacts of bias voltage, ageing, and light on trapping behavior are experimentally investigated and reported through the low-frequency measurement of different GaN technologies such as non-intentionally doped or carbon doped $In_{0.19}Al_{0.81}N$/GaN HEMTs.

This characterization method presents an advantage over the other methods based on pulsed voltage principle (DLTS, etc.) by avoiding pulse effects like voltage stabilization time or non-constant temperature. It also offers a number of key advantages such as its wide dynamic range and

https://doi.org/10.1017/S1759078715000094 Published online by Cambridge University Press

measurement speed. As this method is very sensitive, it reveals some complex behavior of the trapping phenomena. However, we still have to overcome some difficulties such as the weak trap excitation under low fields, the interactions between several detected traps or the extraction of acceptor-like traps.

Given the strong dependency of the extracted activation energy with the applied bias, it is difficult to compare these extracted values with other works. Nevertheless, in further studies, these extracted values of activation energy and capture cross-section can be used within a cycle of physical simulations to assess the possible origin of the detected traps.

The future work on this characterization method is to overcome these drawbacks and improve the measurement interpretations with the help of physical device simulations, in order to provide an efficient feedback to the technological developments.

REFERENCES

[1] Binari, S.C.; Klein, P.B.; Kazior, T.E.: Trapping effects in GaN and SiC microwave FETs, In Proc. of the IEEE, **90** (6) (2002), 1048–1058.

[2] Lang, D.V.: Deep-level transient spectroscopy: a new method to characterize traps in semiconductors. J. Appl. Phys., **45** (7) (1974), 3023–3032.

[3] Gavryushin, V.: Deep level saturation spectroscopy. Int. J. Opt., ID. 505023, **2012** (2012), 1–16.

[4] Jardel, O. et al.: Modeling of Trap Induced Dispersion of Large Signal Dynamic Characteristics of GaN HEMTs, in IEEE/MTT-S Int. Microwave Symp., Seattle, 2013, 1–4.

[5] El Rafei, A. et al.: DC (10 Hz) to RF (40 GHz) output conduction extraction by S-parameters measurements for in-depth characterization of AlInN/GaN HEMTS, focusing on low frequency dispersion effects, in European Microwave Conf. (EuMIC), Manchester, 2011.

[6] Umana-Membreno, G.A. et al.: Low-temperature shallow-trap related output-admittance frequency dispersion in AlGaN/GaN MODFETs, in Conf. on Optoelectronic and Microelectronic Materials Devices, Perth, 1998, 252–255.

[7] Potier, C. et al.: Trap characterization of microwave GaN HEMTs based on frequency dispersion of the output-admittance, in European Microwave Conf., Roma, 2014.

[8] Camacho-Peñalosa, C.; Aitchison, C.S.: Modelling frequency dependence of output impedance of a microwave MESFET at low frequencies. Electron. Lett., **21** (12) (1985), 528–529.

[9] Nsele, S.D.; Escotte, L.; Tartarin, J.G.; Piotrowicz, S.; Delage, S.L.: Broadband frequency dispersion small-signal modeling of the output conductance and transconductance in AlInN/GaN HEMTs. IEEE Trans. Electron Devices, **60** (4) (2013), 1372–1378.

[10] Agilent E5061B Network Analyzer, Agilent data sheet, http://cp.literature.agilent.com/litweb/pdf/5990-6794EN.pdf

[11] Mitrofanov, O.; M. Manfra, M.: Poole–Frenkel electron emission from the traps in AlGaN/GaN transistors. J. Appl. Phys., **95** (11) (2004), 6414–6419.

[12] Kayis, C.; Zhu, C.Y.; Mo, W.; Li, X.; Ozgur, U.; Morkoc, H.: Field-assisted emission in AlGaN/GaN heterostructure field-effect transistors using low-frequency noise technique. J. Appl.Phys., **109** (8) (2011), 084522–084522–5.

[13] Götz, W.; Johnson, N.M.; Bremser, M.D.; Davis, R.F.: A donor like deep level defect in Alo.12Gao.88N characterized by capacitance transient spectroscopies. Appl. Phys. Lett., **69** (16) (1996), 2379–2381.

[14] Jungwoo, J.; DeAlamo, J.A.: Mechanisms for electrical degradation of GaN high-electron mobility transistors, in Int. Electron Devices Meeting, San Francisco, 2006, 1–4.

[15] Azhar Iqbal, M.; Jones, B.K.: A Comparison of the trap properties and locations within GaAs field-effect transistors under different bias conditions. IEEE Trans. Electron Dev., **45** (8) (1998), 1663–1670.

Clément Potier was a graduated Engineer from INSA Lyon, France, in 2012. He is currently working toward his Ph.D. degree at XLIM Laboratory in partnership with the 3–5 Lab. His main fields of interest are the nonlinear characterization and modeling of AlGaN and AlInGaN HEMTs. This requires measurements such as I–V, *S*-parameters, low-frequency *S*-parameters, and load-pull measurements.

Jean-Claude Jacquet received his Engineer degree from the Ecole Supérieure d'Optique, Orsay, France, in 1990. He subsequently joined the Central Research Laboratory of Thales, as a Research Staff Member, where he was involved with spintronic devices. He focused his efforts on the giant magnetoresistive effect and found a new physical effect called the magnetorefractive effect. Since 1999, he has been involved in the development of GaInP HBT and GaN HEMT microwave power devices. He is currently in charge of the thermal management and of the physical modeling aspects of GaN HEMTs at III–V Lab.

Christian Dua received his Engineer degree in Physics from the University of Clermont-Ferrand, France. He joined THOMSON-CSF Group (previous name of THALES) in 1982. He has been working in two different Units of the Group whose main activities were microwave devices (mainly diodes) and optoelectronic components (lasers and LEDs). During this period he gained experience in crystal growth (using several techniques such as Vapor Phase Epitaxy, Liquid Phase Epitaxy, Metal Organic CVD, and Chemical Beam Epitaxy) and physical and electrical characterization of Semiconductor epi-layers and substrates. He is presently working in the SiC activity of the research unit, TRT, and is involved in characterization and assessment of the supplied wafers, and in the study of the reliability of the GaN HEMT technology.

https://doi.org/10.1017/S1759078715000094 Published online by Cambridge University Press

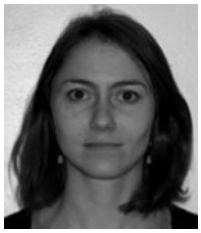

Audrey Martin received her Ph.D. degree from the Limoges University, France, in 2007. She is presently a teacher and researcher with XLIM Laboratory, University of Limoges. Her main research interests include active microwave and millimeter-wave circuit design, wideband power amplifiers, and nonlinear modeling techniques. She is also interested in the development of characterization and modeling of graphene devices.

Michel Campovecchio was born in Angers, France, in 1964. He received his M.S. and Ph.D. degrees in Electrical Engineering from the University of Limoges, France, in 1989 and 1993, respectively. In 1994, he joined the XLIM Institute (formerly IRCOM), Centre National de la Recherche Scientifique (CNRS), Limoges, France, to investigate the nonlinear modeling of high-power microwave transistors and the design of wideband power amplifiers. In 2000, he became a Full Professor with the University of Limoges, where he is in charge of the Power Amplifier Group at XLIM Institute. He is mainly involved in nonlinear modeling and circuit design in III-V and III-N technologies for radar and space applications.

Mourad Oualli was born in France in 1982. He graduated from the Ecole Polytechnique, Palaiseau, France, and from the Ecole Supérieure d'Électricité (Supélec), Gif-sur-Yvette, France, in 2007. The same year he joined the Alcatel-Thales common laboratory III–V Lab as a research engineer for the development of GaN-based HEMT technologies. He especially works on pulsed measurement and DC characterisation as well as on reliability assessment of the devices.

Olivier Jardel received his Engineer degree from University of Aix-Marseille I, in 2004, and the Ph.D. degree from the University of Limoges in 2008, in the common laboratory MITIC between XLIM and III–V Lab. Since 2008, he is a research engineer at III–V Lab and is involved in the development of GaN HEMT power devices. He is in charge of electrical characterizations, transistor modeling, and circuit design.

Stéphane Piotrowicz was born in France 1971. He received his Ph.D. degree in Electronics from the University of Lille in 1999. He Joined the Thales Research Center and worked on the design of Hybrid and MMIC power amplifiers on the InGaP/GaAs HBT technology for Radar and Space Applications. He currently works on the development of GaN technologies at III–V Lab (a joint lab of Alcatel-Lucent Bell Labs France, Thales Research and Technology & CEA Leti). He is in charge of the design and characterization team involved in the realization of hybrid and MMIC circuits for T/R modules as power switches, power amplifiers, and low noise amplifiers.

Sylvain Laurent was born in Chateauroux, France, in 1983. He received his Ph. D. degree in Electronics from the University of Limoges, Brive, France in 2010. He is currently an engineer in the 'Composants Circuits Signaux et Systèmes Hautes Fréquences' department of Xlim laboratory. His research interests include the characterization of RF microwave nonlinear devices.

Raphaël Aubry received the material engineering degree from ECAM Rennes in 1999, the Physic master research degree from the University of Rennes in 2000 and Ph.D. degree from the University of Lille in 2004. His Ph.D. work subject was on the thermal management of the power microwave devices. He joined the THALES research Center and has been working on the development of the power AlGaN/GaN HEMT technology for radar and space applications. He is currently at III–V lab, in charge of the process of GaN based devices.

Olivier Patard received his Engineer degree from INSA Rennes, in 2008, and the Ph.D. degree from INSA Rennes in 2012. His doctoral research, performed at 3–5lab focused on the regrowth by MOVPE of semi-insulating InP for buried optoelectronic heterostructures. His work also includes fabrication and characterizations of advanced photonic integrated circuits on InP for telecommunication. Since 2012, he is a research engineer at III–V Lab in the team microelectronic on GaN. He is involved in the development and the processing of GaN HEMT power devices.

https://doi.org/10.1017/S1759078715000094 Published online by Cambridge University Press

Piero Gamarra received his M.Sc. degree in Physics from the University of Torino, Italy, in 2009, and the Ph.D. degree in material science from the University of Lyon, France, in 2013. His doctoral research, performed at 3–5lab, focused onto the growth by MOVPE of nitride HEMT structures. His work included the growth of AlGaN/GaN and InAlN/GaN HEMT structures on Silicon Carbide for high power amplifiers in S to K-band and in the growth of nitride HEMTs on large area silicon substrates. For these studies, he received the Thales Ph.D. prize 2014.He is currently research scientist in the team of MOVPE epitaxy of wide band-gap materials at 3–5lab. His activities concern the design, the growth and the characterization of advanced heterostructures for III-N semiconductor devices (HEMTs, LED micro-displays and cold cathodes).

Marie-Antoinette di Forte-Poisson is graduated from the Ecole Nationale Supérieure of Physics (Marseille) in 1976 and completed her doctorate in optics at the University of Nice in 1978. In 1978, Dr. di Forte-Poisson joined the Central Research Laboratory of Thomson-CSF and achieved an MBA at the Institut d'Administration des Entreprises (I-A-E, University of Paris) in 1979. Dr. di Forte-Poisson is involved in the MOVPE epitaxy of III–V compounds. She is interested in the growth, characterization and device applications of a variety of ternary compounds. She has authored or co-authored more than 100 papers and several patents. She obtained two Thales awards in 1997 and 2002. Currently, she manages the team responsible for the 'Epitaxial Growth of Wide Band-gap Materials'. She is a Programme Committee Member of the MO-VPE EUROPEAN WORSHOP, the MOVPE International Conference and the International Symposium on Growth on III-Nitrides (ISGN).

Dr. Sylvain L. DELAGE got his Ph.D. at University Paris VII in 1985. His thesis study was focused on the realization of epitaxially grown Si/CoSi2/Si metal base transistors. During his postdoctoral position at IBM T.J. Watson Research Center (Yorktown Heights, NY), he was a member of the team under the leadership of Subramaniam S. Iyer, who demonstrated for the first time the feasibility of SiGe/Si heterojunction bipolar transistor (HBT) in 1987. Since that time, he has been the project leader for the development of the THALES (previously Thomson-CSF) InGaP/GaAs HBT for RF power applications. He is currently leading the III–V Lab Microelectronic group involved in particular in the development of wide bandgap GaN high electron mobility transistors.

Raymond Quéré (Fellow IEEE) received his Electrical Engineering degree from ENSEEIHT (Toulouse France) in 1976 and the French 'Agrégation' in applied physics in 1978. Later he earned the Ph.D. degree from the University of Limoges where he was appointed as Full Professor in 1992. He leads the department of High Frequency Devices, Circuits, Signals and Systems at XLIM Laboratory (CNRS/University of Limoges – France) where he is particularly involved in the modeling and design of nonlinear circuits for Telecommunications and Radar Systems. He authored or co-authored more than 150 publications or communications in international journals and conferences. He co-authored three books and among them a book on the 'Stability of nonlinear microwave circuits'. He is involved in French and European research projects and serves as an expert for the evaluation of research projects for the French Research Agency (ANR).

https://doi.org/10.1017/S1759078715000094 Published online by Cambridge University Press